Article submitted to G4 Journal

Deep geothermal resource assessment of the St. Lawrence Lowlands sedimentary basin (Québec) based on 3D regional geological modelling

Authors and affiliations

Bédard, Karine. Institut national de la recherche scientifique, Centre - Eau Terre Environnement, 490 rue de la Couronne, Québec, QC, G1K 9A9, Canada. karine.bedard@ete.inrs.ca

Comeau, Félix-Antoine. Institut national de la recherche scientifique, Centre - Eau Terre Environnement, 490 rue de la Couronne, Québec, QC, G1K 9A9, Canada. felix-antoine.comeau@ete.inrs.ca.

Raymond, Jasmin. Institut national de la recherche scientifique, Centre - Eau Terre Environnement, 490 rue de la Couronne, Québec, QC, G1K 9A9, Canada. jasmin.raymond@ete.inrs.ca.

Gloaguen, Erwan. Institut national de la recherche scientifique, Centre - Eau Terre Environnement, 490 rue de la Couronne, Québec, QC, G1K 9A9, Canada. erwan.gloaguen@ete.inrs.ca.

Malo, Michel. Institut national de la recherche scientifique, Centre - Eau Terre Environnement, 490 rue de la Couronne, Québec, QC, G1K 9A9, Canada. michel.malo@ete.inrs.ca.

Richard, Marc-André. Hydro-Québec's research institute, IREQ, 600 av. de la Montagne, Shawinigan, Québec, G9N 7N5, Canada. richard.marc-andre@ireq.ca.

Corresponding author

Raymond, Jasmin. Institut national de la recherche scientifique, Centre - Eau Terre Environnement, 490 rue de la Couronne, Québec, QC G1K 9A9, Canada. Telephone: 418-654-2559. Fax: 418-654-2600. Email: jasmin.raymond@ete.inrs.ca.

Abstract

Geothermal resource quantification requires underground temperature and volume information, which can be challenging to accurately assess at the regional scale. The analytical solution for steady-state heat conduction with internal heat generation is often used to calculate temperature at depth, while geological models can provide volume information. Both approaches were originally combined in a single 3D geological model, in which the underground temperature is directly computed, to accurately evaluate geothermal resources suitable for power generation in the St. Lawrence Lowlands sedimentary basin covering 18,000 km^2 in Quebec, Canada, and improve methods for geothermal resource quantification. This approach, used for the first time at such a large scale, allowed to determine the volume of each thermal unit providing a detail assessment of resource depth, temperature and host geological formation. Only 5% of geothermal resources at a temperature above 120 °C that is suitable for power generation were shown to be hosted in the Cambro-Ordovician sedimentary rock sequences at a depth of 4 to 6 km, while 95% of the resource is hosted by the underlying Precambrian basement.

Keywords

Temperature; thermal; heat conduction; geothermal resource; enhance geothermal system.

Nomenclature

Symbols		**Subscripts**	
A	heat generation rate (μW m^{-3})	e	effective or electrical
c	heat capacity (J kg^{-1} K^{-1})	f	final
E	energy (J)	i	entity or initial
e	vertical thickness (m)	n	total number of entities
P	power (W)	PC	Precambrian basement
Q	heat flow (mW m^{-2})	r	rock
s	thermal diffusivity (m^2 sec^{-1})	rec	recoverable
T	temperature (°C)	sed	sedimentary
t	time (sec)	th	thermal
V	volume (m^3)	tot	total
$\Delta T/\Delta z$	geothermal gradient (°C m^{-1})	z	true vertical depths (TVD; m)
η	efficiency (%)	0	at the surface
λ	thermal conductivity (W m^{-1} K^{-1})		
ρ	density (kg m^{-3})		
ϕ	proportion or recovery factor (%)		

1 Introduction

Three-dimensional (3D) modeling is nowadays widely used in regional to site scale geological projects. Geothermal resource assessments are following the trend and making use of different 3D models, both conceptual (e.g. Sausse *et al.*, 2010; Siler *et al.*, 2019) and numerical (e.g. Blöcher *et al.*, 2010; Zhao *et al.*, 2015), just to cite a few examples where models are used to better estimate geothermal system geometry, characteristics and geodynamics. 3D geophysical models based on inversion methods are also used for geothermal exploration and monitoring with magnetotelluric, electrical resistivity, seismic and gravity data to better characterize the subsurface (Newman *et al.*, 2008; Nieto *et al.*, 2019).

Advances in 3D modeling software and computer capabilities are allowing to create large 3D geological models and calculate temperature at depth based on heat transfer mechanisms. Moreover, as the geometry of the subsurface is modelled in 3D, the volume and distribution of the geothermal targets can be evaluated more accurately, which is one step forward in the assessment of the geothermal potential of a region. However, 3D geological models are not commonly used for estimating geothermal resources at the regional or basin scale. Relatively small-scale 3D geothermal models, on the order of ≤100 km in diameters, are described in the literature with non-exhaustive examples from around the world including Denmark, Germany, Iceland, Italy, New Zealand, The Netherlands, the United States of America and Taiwan (e.g. Guglielmetti *et al.*, 2013;; Chang *et al.*, 2014; Gasperikova *et al.*, 2015; Ratouis *et al.*, 2016; Siler *et al.*, 2016; Przybycin *et al.*, 2017; Békési et al., 2020; Fuchs, 2020). On the other hand, regional or large-scale 3D models, on the order of >100 km diameters, are just starting to be used for the assessment of geothermal resources. Recent examples of interest include the shallow geothermal potential assessment related to ground source heat pumps by Santilano *et al.* (2016) in Italy and the basin-scale deep geothermal potential evaluation for the French Massif Central by Calcagno *et al.* (2014), Central Alberta in Canada by Hofmann *et al.* (2014) and the Williston Basin in the United States of America by Gosnold *et al.* (2016). How to properly develop such 3D regional geological models and implement heat transfer equations to accurately evaluate temperature for estimating deep geothermal resources remain challenging. Large-scale geothermal resource assessments tend to be conducted in 2D (Blackwell *et al.*, 2006; Batir *et al*., 2016; Stutz *et al.*, 2015; Palmer-Wilson *et al.*, 2018), where only surface heat flow estimation is used to extrapolate temperature downward. In this study, an example of 3D geothermal resource assessment for the St. Lawrence Lowlands (SLL) sedimentary basin in Québec, Canada, is provided using a geological model covering an area of 230 by 75 km to address this challenge. The study illustrates how 3D geological modeling can be originally combined with thermal characterization of stratigraphic units to extrapolate temperature at depth using analytical solutions, considering the basin complex geometry, to properly estimate deep geothermal resources. We believe this new 3D approach allows to better identify geothermal targets with appropriate volume information compared to a conventional 2D approach.

Previous geothermal studies of the SLL basin in southern Québec relied on raw and/or corrected bottom-hole temperature (BHT) data obtained from oil and gas exploration wells combined with rock thermal conductivity inferred from the literature (SNC-SOQUIP, 1979; e.g. Lefebvre et Trempe, 1980; Majorowicz et Minea, 2012; Raymond *et al*., 2012; Majorowicz et Minea, 2015b) to estimate temperature at depth. Recent works allowed to present one-dimensional analysis of the geothermal state of the basin by defining thermal conductivity, heat generation and temperature at depth evaluated by physical measurements of thermal properties of each stratigraphic unit (Bédard *et al.*, 2017; Nasr *et al*., 2018). The current manuscript follows previous work from Bédard *et al.* (2017) in order to evaluate subsurface temperature in the 3D space as a further step, providing the missing volume information to calculate the actual geothermal resource potential of the SLL basin. The new method developed in this work allows obtaining accurate volume information to quantify and localize in the subsurface the thermal energy content that can be converted to sustainable electricity. The original 3D geological model of the SLL basin (Bédard *et al.*, 2013) was a key to determine this missing volume information, moving toward a first complete resource quantification integrating in a novel fashion analytical heat transfer solutions in such a regional model. The use of a large-scale 3D geological model as a support for heat transfer calculations to obtain a detailed estimate of the temperature at depth is a significant advance for regional geothermal resource evaluation as it can be used to identify energy content of specific geological formations with complex geometries, which can be difficult to achieve in 2D.

2 Study area

The study area of this project covers 18,000 km^2 in the southern part of the province of Québec, where most of the population lives and hence has significant market potential for deep geothermal resources development. This region also hosts parts of the strongest Canadian market for shallow geothermal installations (Canadian GeoExchange Coalition, 2012). The area is actually located in the SLL sedimentary basin and partly in the Appalachian basin to the south (Figure 1). The SLL basin unconformably overlies the Canadian Shield and is covered by the Appalachian basin in the southeast. The SSL basin deepens toward the southeast because of the presence of NE-SW trending normal faults as shown in Figure 2 (Konstantinovskaya *et al.*, 2009; Castonguay *et al.*, 2010). Most of the normal faults only displaced the upper part of the Canadian Shield, also named the Precambrian basement, and the lower part of the SSL sedimentary sequence as shown in Figure 2.

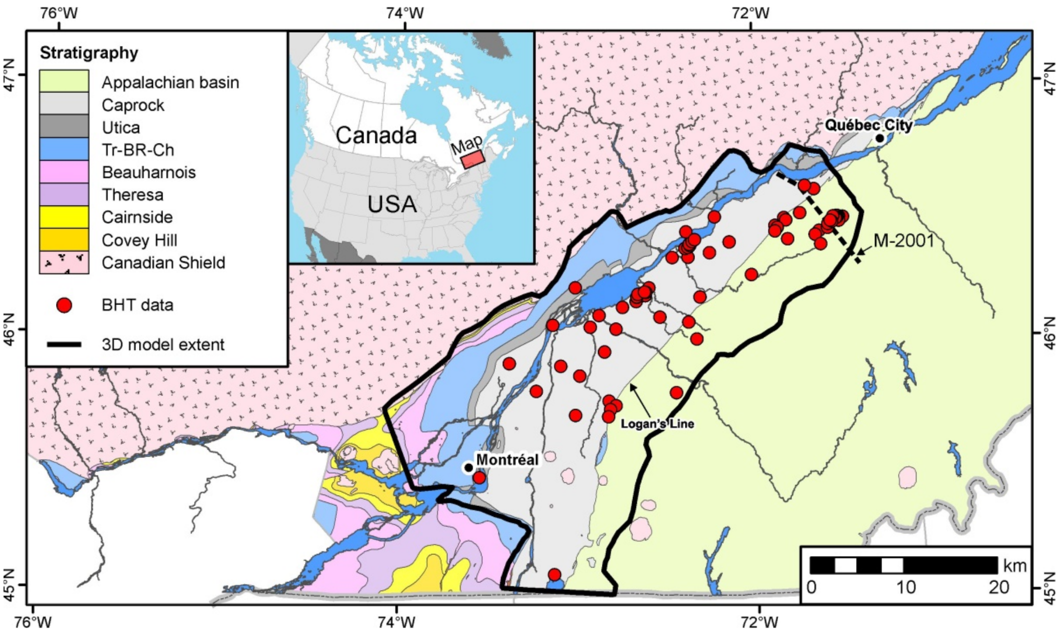

Figure 1. Geological map of southern Québec province showing the thermal units, the extent of the 3D model and BHT data used in this study. The black dashed line shows the location of M-2001 seismic line (Figure 2).

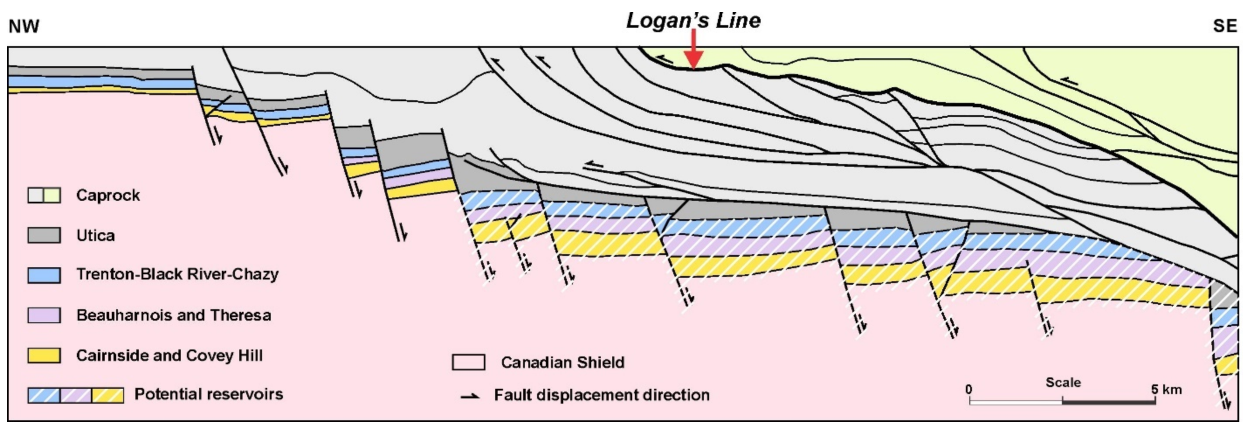

Figure 2. SLL sedimentary basin architecture and thermal units based on M-2001 seismic line with ~2X vertical exaggeration. Modified from Castonguay *et al.* (2010). See Figure 1 for location.

This manuscript uses the concept of thermal units that are defined as consecutive geological layers of similar thermal conductivity and heat generation rate. Considering that thermal properties of rocks are strongly linked to their physical properties, the SLL basin is divided in seven thermal units (Bédard *et al.*, 2017; Raymond *et al.*, 2017) based on the standard lithostratigraphy of the SLL basin proposed by Comeau *et al.* (2013), with one more thermal unit used to represent the Canadian Shield or the Precambrian basement (Figure 1; Figure 2; Table 1).

The Caprock thermal unit is composed of the Queenston, Lorraine and Sainte-Rosalie groups as well as the rocks from the Appalachian basin. The Cambro-Ordovician Appalachian basin is composed of various deformed sedimentary rocks that are not differentiated in the 3D model used in this study. The sedimentary rocks of the Caprock unit are composed of fine-grained siliciclastics, carbonates and shales acting as caprocks with low permeability and potential thermal blanket with relatively low thermal conductivity (Table 1). Underlying carbonate rocks of the Trenton-Black River-Chazy (Tr-BR-Ch) unit are grouped in a single thermal unit in the 3D model because their physical and thus thermal characteristics are similar. The Beauharnois and Theresa units are composed of dolostones grading to dolomitic sandstones and show higher thermal conductivity, with a low matrix porosity on the order of 1~2 % (Tran Ngoc *et al.*, 2014). However, the secondary porosity of the Beauharnois and Theresa units can reach up to 15 % in dolomitic facies due to dissolution along fractures (Bertrand *et al.*, 2003). The clastic rocks of the Cairnside and Covey Hill thermal units show the highest thermal conductivity due to their important quartz content (Table 1). The Canadian Shield is made up of Precambrian igneous, volcanic and metamorphic rocks that are not differentiated in the 3D model and are thus considered as a uniform thermal unit (PC) in this study. With their position at the base of the sedimentary sequence where temperature is higher and because of their potentially higher permeability, the Covey Hill and Cairnside thermal units as well as the fractured basement rocks just below the basin are the principal targets for hydrothermal resources in the SLL basin. The Covey Hill and Cairnside units have a porosity between 4 to 6 % and values that can locally exceed 10 % (Tran Ngoc *et al.*, 2014). Enhanced geothermal systems (EGS) is further considered for the Canadian Shield deep below the basin (Majorowicz and Minea, 2015a).

The input parameters presented in Table 1 were used to estimate the 3D subsurface temperatures of the SLL basin in this study and are described with more detail in Bédard *et al.* (2017). This previous study defined the thermal conductivity and heat generation rate of the different thermal units based on rock sample measurements conducted in the laboratory and on well log analysis (Nasr *et al.*, 2015; 2018). The basement PC unit was sampled North of the basin where the unit crops out and in rare boreholes that reached this unit in order to define thermal properties below the basin and extrapolate temperature at depth. The input temperature data were corrected for both drilling disturbance and paleoclimatic variations in order to estimate the surface heat flow associated with BHT locations (Bedard *et al.*, 2014). It is important to note that deep geothermal resources exploration in the SLL is at an early stage and, as a consequence, there is no equilibrium temperature data available below ~300 m depth. The 81 BHT data used in this study were recorded at a depth varying from 660 to 4,329 m (Figure 1). The estimated equilibrium geothermal gradient taking into account the above corrections ranges from 12.2 to 40.4 °C, with an average of 24.3 ± 4.9 °C km^{-1} (Bédard *et al.*, 2017). Temperature predictions below the deepest borehole, made with the methodology described below, mostly relied on the surface outcrops of the analysed PC unit used as analogues of the deep subsurface.

Table 1. Characteristics of the SLL basin thermal units. Caprock data include the Sainte-Rosalie, Lorraine and Queenston groups as well as the Appalachian basin. Tr-BR-Ch: Trenton-Black River-Chazy unit.

Age		Thermal unit	Lithology	Thermal conductivity [a] ($W\ m^{-1}\ K^{-1}$)	Heat generation rate [a] ($\mu W\ m^{-3}$)	Heat capacity [b] ($J\ kg^{-1}\ K^{-1}$)	Rock density [a,b] ($kg\ m^{-3}$)
ORDOVICIAN	**U**	**Caprock**	*Shales Siltstones Sandstones Limestones*	2.79 ± 0.75	1.59 ± 0.28	890	2,700
ORDOVICIAN	**U**	**Utica**	*Black calcareous shale*	2.52 ± 0.31	0.95 ± 0.37	832	2,450
ORDOVICIAN	**U** / **M**	**Tr-BR-Ch**	*Limestones Shaly limestones*	2.85 ± 0.46	0.41 ± 0.27	852	2,700
ORDOVICIAN	**M** / **L**	**Beauharnois**	*Massive dolostones*	3.80 ± 0.62	0.69 ± 0.27	862	2,740
ORDOVICIAN	**L**	**Theresa**	*Sandy dolostones*	4.29 ± 1.44	0.94 ± 0.30	847	2,705
CAMBRIAN	**U**	**Cairnside**	*Quartzitic sandstones*	6.19 ± 0.60	0.25 ± 0.14	827	2,650
CAMBRIAN	**U** / **M**	**Covey Hill**	*Feldspathic sandstones Conglomerates*	4.78 ± 1.22	0.79 ± 0.28	796	2,630
PC		**Canadian Shield**	*Igneous, volcanic and metamorphic*	3.00 ± 0.78	N/A	762	2,598

[a] Data source: Bédard *et al.* (2017) and references therein. [b] Data source: Nasr *et al.* (2015); Nasr (2016).

3 Methodology

This study aims at estimating the 3D subsurface temperature of the SLL basin and the underlying basement, up to 13 km, with the use of a 3D geological model in which thermal properties are distributed respecting the 3D geometry of the thermal units at depth. The basin deep temperature is then used to assess the geothermal resource base according to the methodology used by MIT (2006). Both resources associated to the basement with potential for EGS technologies and associated to the basal sedimentary units that can host natural reservoirs are considered although most of the resource that can be used for power generation is located in the basement.

3.1 Temperature at depth

The 3D geological model of the SLL basin, previously constructed with the GOCAD software and presented by Bédard *et al.* (2013), was used as the basis for the 3D temperature assessment of the basin. In the model, the geological map of the area defines the location of rock units at surface and was combined with a structural map of the Precambrian basement top in two-way travel time units converted to depth with well data to further constrain the geometry and depth of the Precambrian basement. Geophysical well logs from 81 oil and gas exploration wells were reinterpreted and used to determine the elevation of rock unit contacts to provide an extensive dataset with a total of 441 contact locations and built the 3D geological model. The location of major faults was defined according to the map of the Precambrian basement depth and differences in elevation between the rock unit contacts in wells. Some modifications to the initial model were achieved to comply with the geothermal assessment objective. The original model was extended toward the southeast to include more data and take possible temperature anomalies into account. The 3D model was also extended to a depth of 13 km, which meant to extend the PC thermal unit downward. Each 3D cell of the model has a distinct thermal conductivity, heat generation rate, thermal capacity and rock density that are defined according to the thermal unit in which the cell belongs. This allows having a more realistic distribution of the parameters in the 3D space as a function of the thermal unit depth and thickness that vary in the basin. This study assumes a purely vertical conductive heat transfer in the basin. The analytical solution for steady-state heat conduction with internal heat generation was actually implemented in the GOCAD software to evaluate temperature at depth. Moreover, because of the lack of sufficient data to estimate spatial distributions of the parameters, thermal conductivity and heat generation rates are both defined as homogeneous in each thermal unit and then, do not vary with depth, temperature or location.

Effective thermal conductivity and heat generation rate are calculated assuming that heat flow is vertical. The effective thermal conductivity λ_e is calculated cell by cell directly in the 3D model with a harmonic mean of the thermal conductivity from the surface downward following the equation:

$$\frac{1}{\lambda_e} = \sum_{i=1}^{n} \frac{\phi_i}{\lambda_i} \qquad (1)$$

where λ_i (W m^{-1} K^{-1}) is the thermal conductivity of the *i*-cell and ϕ_i (%) is the thickness proportion of the *i*-cell compared to the total thickness from the *n*-cell to the surface.

The effective heat generation rate A_e is calculated cell by cell in the 3D model with a weighted arithmetic mean of the heat generation rate from the surface downward following the equation:

$$\boldsymbol{A}_{\mathbf{e}} = \frac{\sum_{i=1}^{n}(A_i \cdot e_i)}{\sum_{i=1}^{n} e_i} \qquad (2)$$

where e_i (m) is the thickness of the *i*-cell with the given heat generation rate A_i (W m^{-3}).

The distribution of the surface heat flow has been interpolated for the entire SSL basin using 81 surface heat flow values $Q_{0,P50}$ calculated from deep corrected BHTs (Bédard *et al.*, 2017). Simple kriging (SK) was used to spatialize the Q_0 values over the entire area of the model. This method is well known for interpolating sparse continuous properties, while considering spatial correlation (Srivastava, 1994). The experimental variogram was calculated on raw data and the variogram was best modelled by a spherical function with a range of 40 km, a sill of 1 and a nugget effect of 40%.

The temperature of sedimentary rock units is calculated cell by cell directly in the 3D geological model from the surface downward by using the linear decrease relationship theory that characterizes the internal heat generation, with the following equation implemented in GOCAD (e.g. Jessop, 1990; Stein, 1995; Turcotte and Schubert, 2014):

$$\boldsymbol{T}_{\mathbf{z(sed)}} = \boldsymbol{T}_{\mathbf{0}} + \left(\frac{Q_0 \cdot z_{\mathrm{sed}}}{\lambda_{\mathrm{e,z}}}\right) - \left(\frac{A_{\mathrm{e,z}} \cdot z_{\mathrm{sed}}^2}{2\lambda_{\mathrm{e,z}}}\right) \qquad (3)$$

where $T_{z(sed)}$ (°C) is the temperature at depth *z* in the sedimentary rocks; T_0 is the average surface temperature (8°C); Q_0 (W m^{-2}) is the surface heat flow; z_{sed} (m) is the depth in the sedimentary rocks; $\lambda_{\mathrm{e,z}}$ (W m^{-1} K^{-1}) is the effective thermal conductivity at depth *z*; and $A_{\mathrm{e,z}}$ (W m^{-3}) is the average heat generation rate at depth *z*.

The exponential decrease relationship theory, developed by Lachenbruch (1970), is used in this study to extrapolate temperature at depth of the Canadian Shield thermal unit cell by cell from the top to bottom, using the following equation in GOCAD (e.g. Jessop, 1990; Turcotte and Schubert, 2014):

$$\boldsymbol{T}_{\mathbf{z(PC)}} = \boldsymbol{T}_{\mathbf{PC}} + \left(\frac{\boldsymbol{Q}_{\mathbf{PC}} \cdot \boldsymbol{z}_{\mathbf{PC}}}{\boldsymbol{\lambda}_{\mathbf{PC}}}\right) - \left(\frac{\boldsymbol{A}_{\mathbf{PC}} \cdot \boldsymbol{e}_{\mathbf{PC}}{}^{\mathbf{2}} \cdot \left[\mathbf{1} - \mathbf{exp}\left(-\frac{\boldsymbol{z}_{\mathbf{PC}}}{\boldsymbol{e}_{\mathbf{PC}}}\right)\right]}{\boldsymbol{\lambda}_{\mathbf{PC}}}\right) \quad (4)$$

where $T_{z(PC)}$ (°C) is the temperature at depth in the Precambrian; T_{PC} (°C) is the temperature at the top of the Precambrian; Q_{PC} (W m^{-2}) is the calculated heat flow at the top of the Precambrian; z_{PC} (m) is the depth from the top of the Precambrian; λ_{PC} (W m^{-1} K^{-1}) is the thermal conductivity of the Precambrian; A_{PC} (W m^{-3}) is the heat generation rate of the Precambrian; and e_{PC} (m) is the total thickness of the Precambrian considered in the 3D model. The use of the two different equations to calculate the temperature in the sedimentary succession and in the Precambrian basement is still debated in the scientific community and can difficultly be confirmed (Turcotte and Schubert, 2014). Equation (2) was used to take into account the heat generation of the radiogenic elements assumed to be uniform in each sedimentary rock unit (Equation 3) and to decrease exponentially in the igneous and metamorphic rocks of the basement (Equation 4). This approach to calculate temperature at depth takes into account the different nature of the sedimentary versus crystalline rock of the basement. The base of the 3D model is set to 13 km to perform the downward temperature extrapolation taking into account the thickness of the sedimentary sequence as proposed by Blackwell *et al.* (2006). The calculation of A_{PC} and e_{PC} developed in Bédard *et al.* (2017) are used in this paper in order to get the values of those parameters. It must be noted that heat generation rate of the Precambrian A_{PC} is assumed to be constant at depth for each location. Consequently, this approach results in an adjustment of the heat generation rate of the Precambrian A_{PC} for each location based on the corrected input temperature data and assuming a constant mantle heat flow of 15 W m^{-2} (Bédard *et al.*, 2017). Therefore, thermal anomalies recorded in oil and gas exploration wells are assumed to be caused by variations of concentration of radiogenic elements in the underlying Precambrian thermal unit. Input temperature data used at this point have been previously corrected for paleoclimate variation to estimate heat flow further used to extrapolate the theoretical undisturbed temperature in the absence of paleoclimate perturbations. The paleoclimate correction is thus removed as a last step from the calculation of extrapolated temperature in order to obtain an estimate of the actual subsurface temperature.

3.2 Geothermal resources

The subsurface temperature being assessed, the estimation of the geothermal resources was then achieved with the 3D model calculating the thermal energy in place or heat volume (i.e. MIT, 2006; Williams *et al.*, 2008). The use of the 3D model allows to directly calculate an accurate volume of each thermal unit with geothermal potential at depth based on the exact basin geometry that is fairly complex. In the case of the SLL, calculations have been achieved on 1 km thick layers from 3 to 10 km depth for temperature ranges of 120 to 150 °C and more than 150 °C. Moreover, the use of the 3D model allowed estimating the resources for three different geological entities: 1) all the potential reservoir units of the sedimentary sequence from the Tr-BR-Ch to the Covey Hill thermal units; 2) the Cairnside and Covey Hill only; and 3) the Canadian Shield (PC unit). The assessment of the total geothermal energy content E_{tot} (J) is calculated with:

$$E_{\mathrm{tot}} = \rho \cdot c \cdot V_{\mathrm{r}} \cdot (T_{\mathrm{i}} - T_0) \qquad (5)$$

where ρ (kg m^{-3}) is the rock density; c (J kg^{-1} °C^{-1}) is the heat capacity; V_r (m^3) is the rock volume; T_i (°C) is the initial rock temperature; and T_0 (8°C) is the average surface temperature.

Following the method used by MIT (2006), the recoverable energy is constrained by a recovery factor that was set to 2 and 20 % (pessimistic and optimistic heat recovery scenarios), as well as by the reservoir temperature drop that is limited to 10 °C in order to keep sustainable reservoir conditions during system operation. The recoverable energy was thus calculated with:

$$E_{\mathrm{rec}} = E_{\mathrm{tot}} \cdot \frac{(T_{\mathrm{i}} - T_{\mathrm{f}})}{(T_{\mathrm{i}} - T_0)} \cdot \phi \qquad (6)$$

where E_{rec} (J) is the recoverable geothermal energy; E_{tot} (J) is the total geothermal energy content; T_i (°C) is the initial rock temperature; T_f (°C) is the final rock temperature; T_i-T_f (10 °C) is the maximum reservoir temperature drop; T_0 (8 °C) is the average surface temperature; and ϕ (%) is the recovery factor.

Once the recoverable geothermal energy is determined, it is finally converted in useful energy, which is electricity in this case, where it is estimated in the context of a binary power plant with an operation period of 30 years. The recoverable electric power is calculated following:

$$P_{\mathrm{e}} = \frac{E_{\mathrm{rec}} \cdot \eta_{\mathrm{th}}}{t} \qquad (7)$$

where P_e (J s^{-1} or W) is the electrical power; E_{rec} (J) is the recoverable geothermal energy; η_{th} (%) is the thermodynamic efficiency and t (sec) is the exploitation lifetime. For typical binary power plant, in which the geothermal fluid temperature is between 100 and 165 °C (MIT, 2006), the net thermodynamic efficiency is:

$$\eta_{\mathrm{th}} = (0{,}0935 \cdot T_{\mathrm{i}}) - 2{,}3266 \quad (8)$$

where η_{th} (%) is the thermodynamic efficiency and T_i is the initial rock temperature (°C).

4 Results

4.1 Temperature at depth

The size of the SLL basin 3D model used in this study is 240 x 130 km by 13 km thick with cells of 753 x 1,004 m by 10 m thickness. The long axis of the model is oriented SW-NE to comply with the anisotropic geometry of the basin. The 3D model includes 30,239,173 cells that are grouped in eight thermal units (Figure 3A and B).

As shown in Figure 3C and E, both the thermal conductivity and the heat generation rate are constant in each of the eight thermal units. The use of the 3D model allows calculating the effective thermal conductivity and heat generation rate at depth taking into account the 3D geometry of the units at the basin scale (Figure 3D and F).

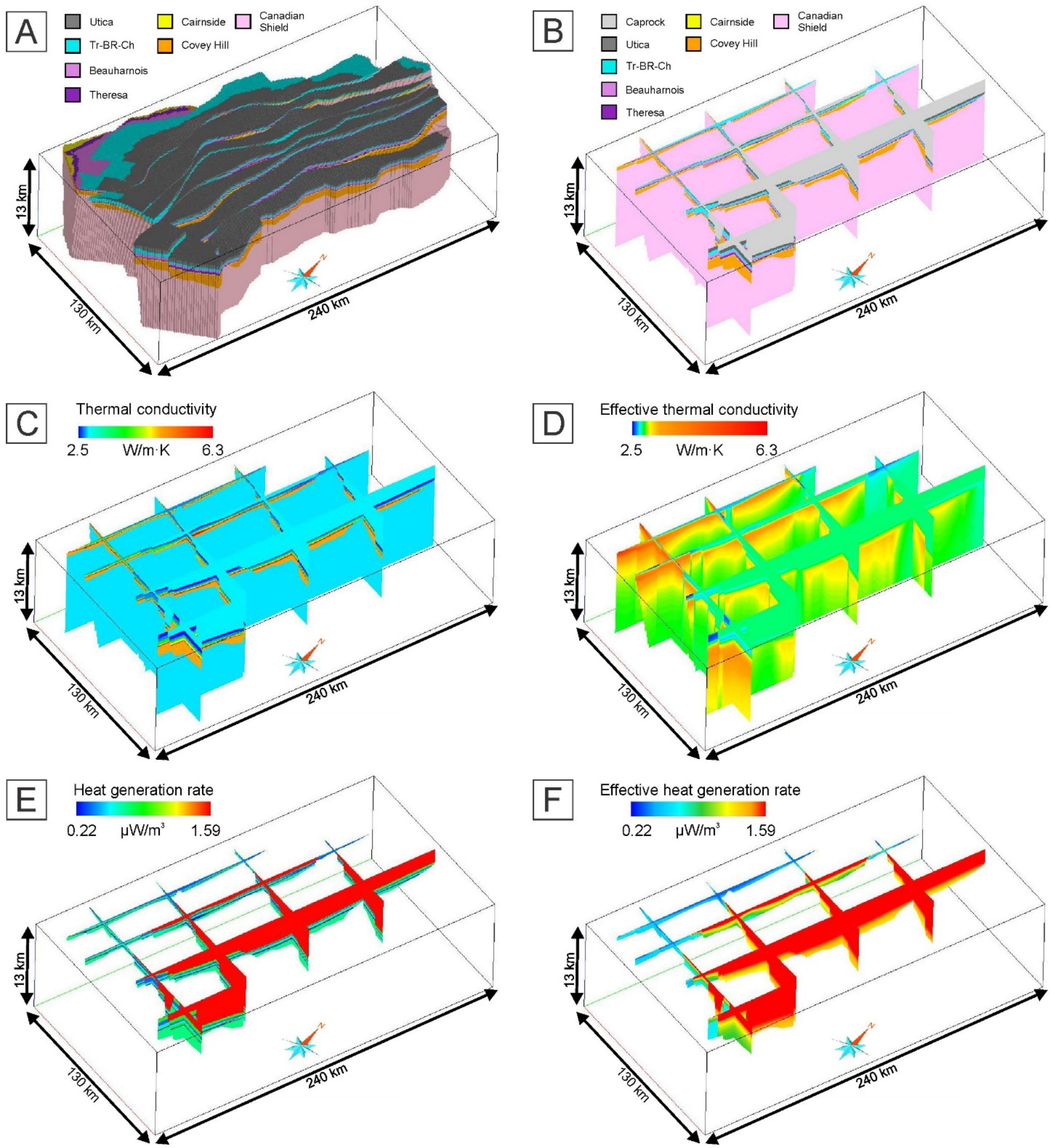

Figure 3. 3D geological model of the SLL basin with thermal units and their properties. (A) Volume model without the Caprock thermal unit. Vertical cross-sections showing (B) the architecture of the 3D model, the 3D distribution of (C) the thermal conductivity, (D) the effective thermal conductivity, (E) the heat generation rate for the sedimentary sequence and (F) the effective heat generation rate for the sedimentary sequence. Vertical exaggeration: 5X.

The surface heat flow is mapped with kriging in Figure 4 and its associated standard deviation is shown in Figure 5. The kriging map of the heat flow highlights 2 positive heat flow anomalies aligned North-South along the south shore of St. Lawrence river and a low trend along north shore. The main goal here was not to obtain an accurate surface heat flow map from equilibrium temperature data since appropriate equilibrium temperature profiles for deep wells are not available in the SLL basin such that basin scale heat flow can only be estimated from BHT data. Important uncertainty consequently remains about heat flow distribution in the basin. Accordingly, this surface heat flow map can be seen as an intermediate step in the methodology to compute the 3D temperature distribution at depth. It is strictly dependent on the input BHT data, but this does not affect the 3D approach presented in this manuscript. Geothermal exploration in the SLL basin is at an early stage and equilibrium temperature data can be integrated as it will become available when geothermal exploration moves to further steps. Thereby, the heat flow assessment can difficultly be compared to previous and actual heat flow maps of the study area, which rely on shallow wells with equilibrium temperature data and commonly tend to display lower values of heat flow for the region (e.g. Saull *et al.*, 1962; Mareschal *et al.*, 1989; Guillou-Frottier *et al.*, 1995; Blackwell et Richards, 2004; Majorowicz et Minea, 2012).

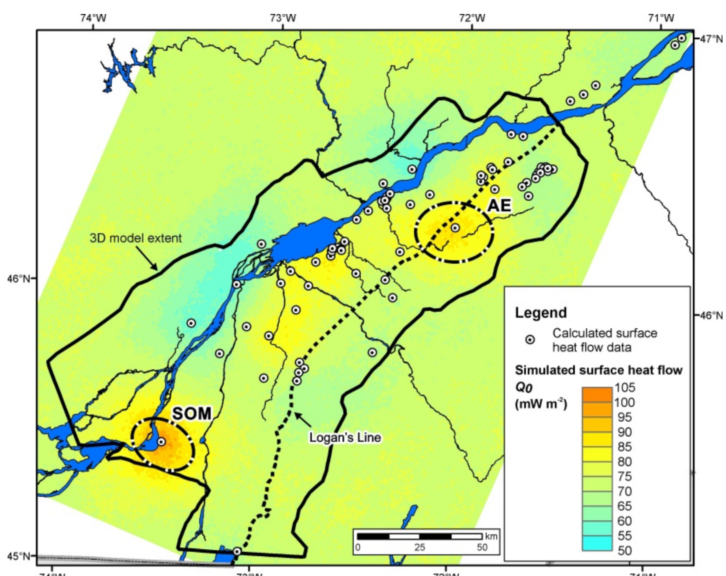

Figure 4. Distribution of surface heat flow of the SLL basin generated by kriging surface heat flow estimated at oil and gas exploration wells. Black ellipses show the positive anomalies of the surface heat flow. SOM: *Southeast of Montreal* anomaly. AE: *Arthabaska-Érable* anomaly.

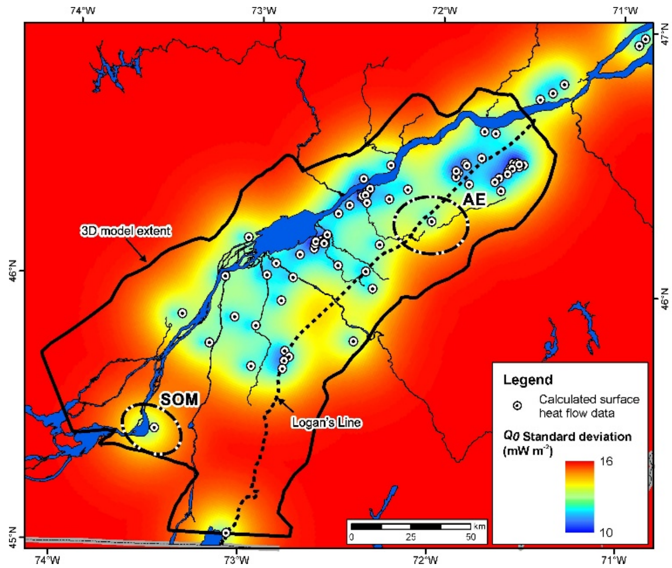

Figure 5. Standard deviation associated to surface heat flow kriging.

The 3D subsurface temperature distribution is calculated from previously defined parameters until the base of the sedimentary sequence. The temperature at the base of the sedimentary sequence is then used to evaluate the heat generation rate of the Precambrian A_{PC} (Figure 6). The anomalies in the heat generation rate of the Precambrian thermal unit are related to the surface heat flow anomalies shown in Figure 4. It is therefore assumed that anomalies in heat generation rate and surface heat flow are caused by varying concentration of radiogenic elements in the underlying Canadian Shield (PC unit).

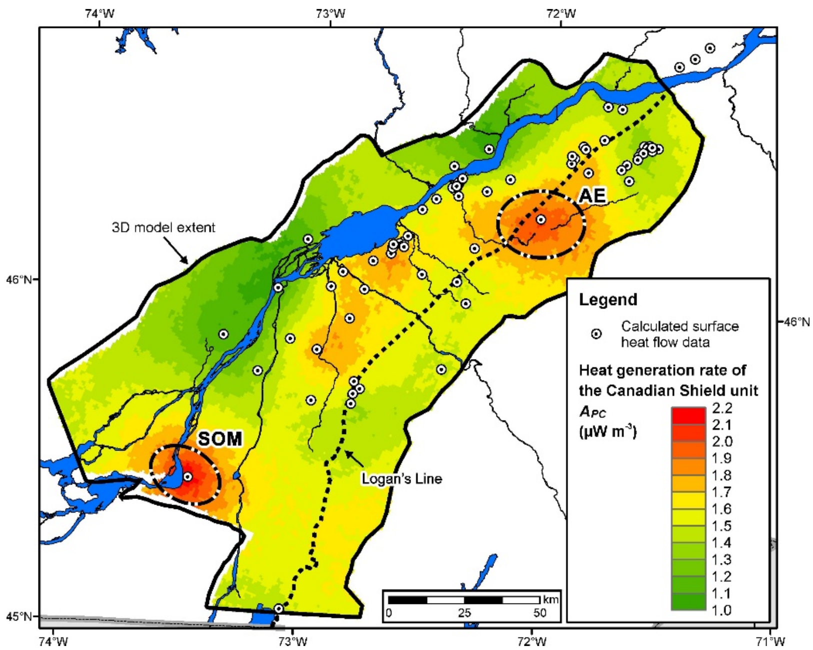

Figure 6. Distribution of heat generation rate calculated for the Canadian Shield thermal unit. Black ellipses show the positive anomalies of the surface heat flow. SOM: *Southeast of Montreal* anomaly. AE: *Arthabaska-Érable* anomaly.

Finally, the temperature in the Precambrian basement is calculated and merged with the sedimentary sequence temperature while reprocessing for the paleoclimate correction in order to provide a complete 3D subsurface temperature model of the SLL at present time (Figure 7). The calculated temperature varies from 8 °C at the surface to 150 °C at 5 km depth and 300 °C at 10 km depth in the anomalies of *Southeast of Montreal* (SOM) and *Arthabaska-Érable* (AE; Figure 8). The SOM anomaly is constrained by one BHT data point only while wells surrounding the AE anomaly suggest a stronger heat flow that peaks toward the well with higher BHT.

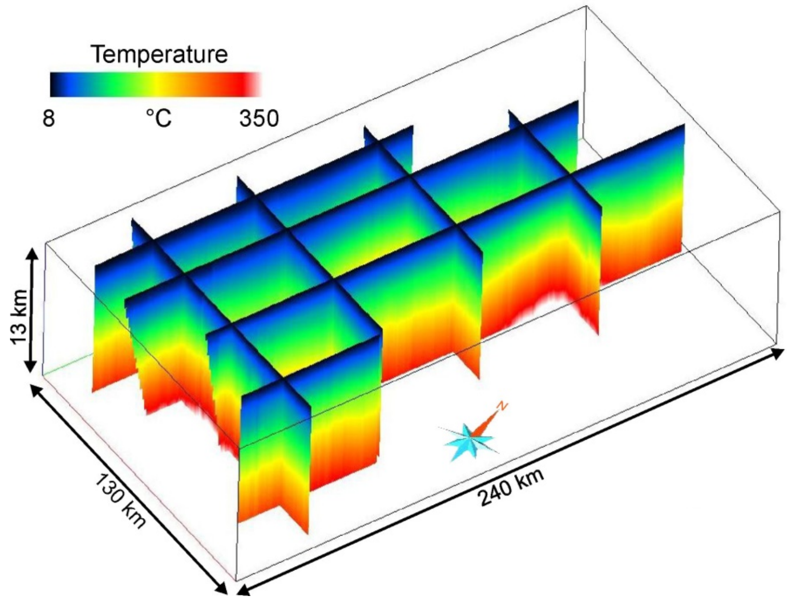

Figure 7. Cross-sections view of the calculated subsurface temperature in the SLL basin and the underlying Canadian Shield.

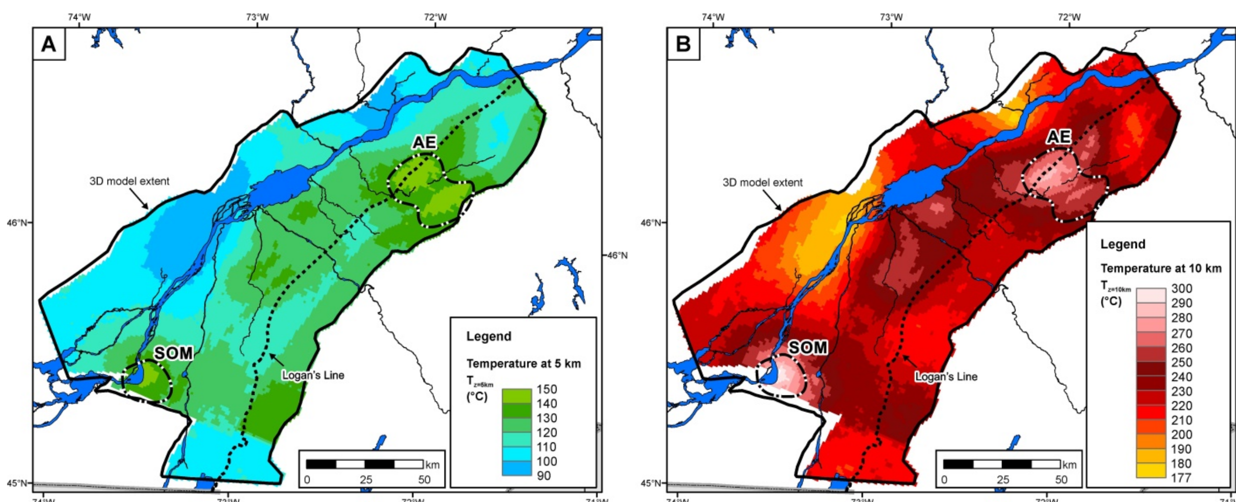

Figure 8. Calculated subsurface temperature at A) 5 km depth and B) 10 km depth. SOM: *Southeast of Montreal* anomaly. AE: *Arthabaska-Érable* anomaly.

4.2 Geothermal resources

The use of the 3D model allowed to compute the total amount of thermal energy that can be recovered from each unit, some sedimentary units having reservoir potential while the Precambrian basement is mostly associated to EGS. Threshold temperatures of 120 and 150 °C have been used to assess geothermal resources for power generation. The depth at which 120 °C is found is between 3,700 and 6,800 m, with an average of 5,200 m, while the shallower depth is located to the AE anomaly (Figure 9A). A temperature of 150 °C is reached between 5,000 and 8,500 m depth, with an average of 6,500 m and the shallowest depth in the AE and SOM anomalies (Figure 9B). The units with geothermal potential having temperature between 120 and 150 °C are thus located between 3 and 9 km depth (Figure 10A) and reach a maximum thickness of 2,000 m. Units with temperature higher than 150 °C are found between 5 and 10 km depth (Figure 10B). The SSL sedimentary basin thickness at the location of the SOM temperature anomaly is less than 1,800 m such that a temperature greater than 120 °C is found in the Canadian Shield thermal unit only. Temperature above 120 °C in the AE anomaly is found both in the SSL thermal units with potential reservoir characteristics and in the Precambrian thermal unit. The SSL basin in the northern part of the AE anomaly is in the 120-150 °C temperature range with an average thickness of 925 m (975 m for the combined Cairnside and Covey Hill thermal units) while the SSL basin above 150 °C has an average thickness of 1,170 m (700 m for the combined Cairnside and Covey Hill thermal units) in the southern part of the anomaly.

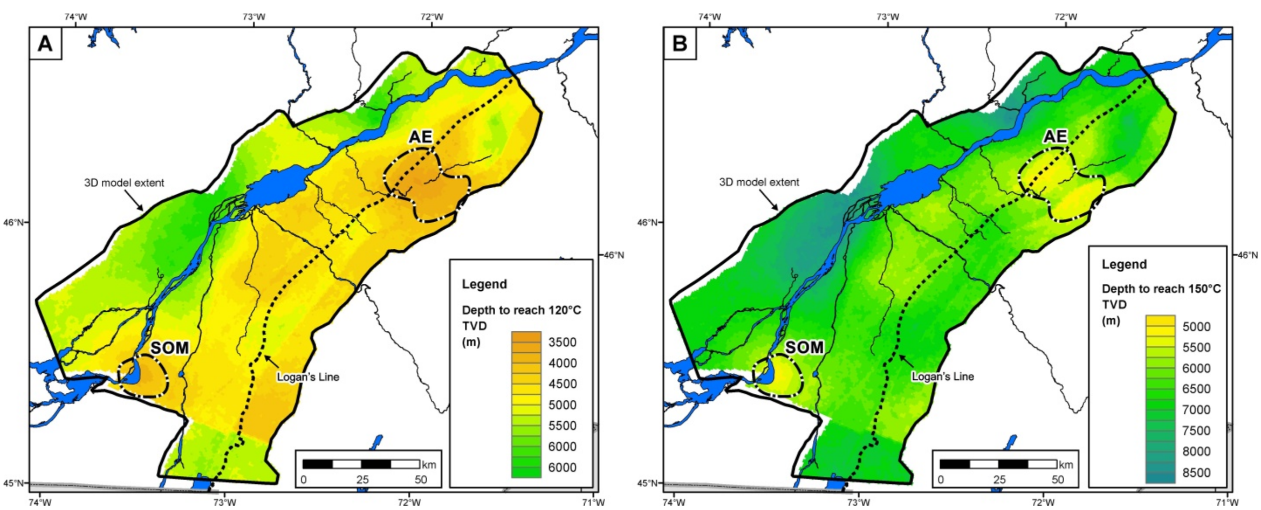

Figure 9. A) Depth to reach 120 °C. B) Depth to reach 150 °C. SOM: *Southeast of Montreal* anomaly. AE: *Arthabaska-Érable* anomaly. TVD: True Vertical Depth.

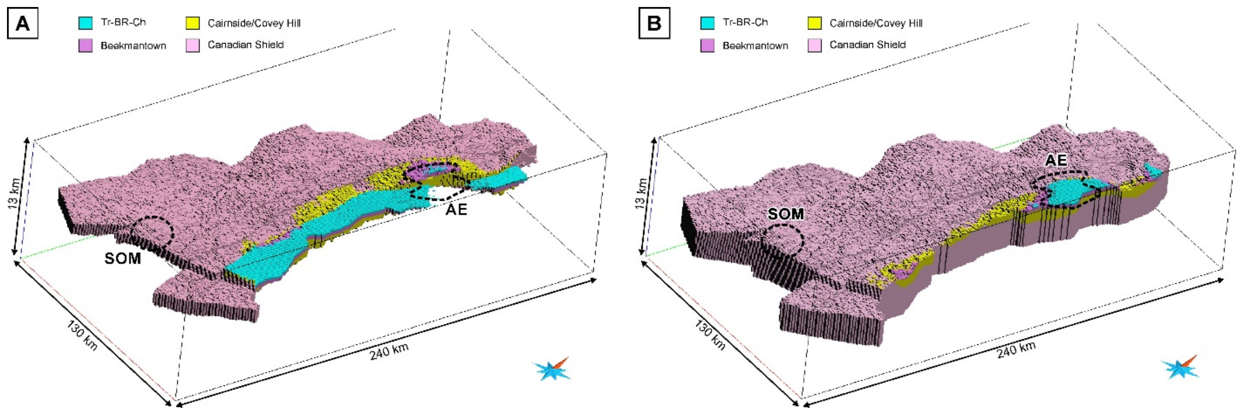

Figure 10. 3D geological model showing thermal units A) between 120 and 150 °C and B) above 150 °C and down to 10 km depth. SOM: *Southeast of Montreal* anomaly. AE: *Arthabaska-Érable* anomaly.

The total geothermal energy (eq. 5) present in all thermal units, including the Canadian Shield, with temperatures above 120 °C and down to 10 km is in the order of 25,000 EJ. The total recoverable geothermal energy (eq. 6) of the SSL basin is in the order of 320 EJ and 32 EJ, when considering recovery factors of 20% and 2%, respectively (Figure 11). About 95 % of this energy is contained in the Canadian Shield (PC unit), which also represents the most important volume among all thermal units between 3 and 10 km depth (Figure 12). The geothermal energy present in the SSL basin is mostly available between 4 and 7 km depth at temperatures between 120 and 150 °C. The geothermal energy contained in the combined Cairnside and Covey Hill thermal units with potential reservoir characteristics contains the greater proportion of the energy among the sedimentary rock units. Geothermal resources with temperature above 150 °C in the combined Cairnside and Covey Hill thermal units is mainly available between 6 and 7 km depth and is on the order of 3 and 0.3 EJ when considering a 20% and 2% recovery factor, respectively.

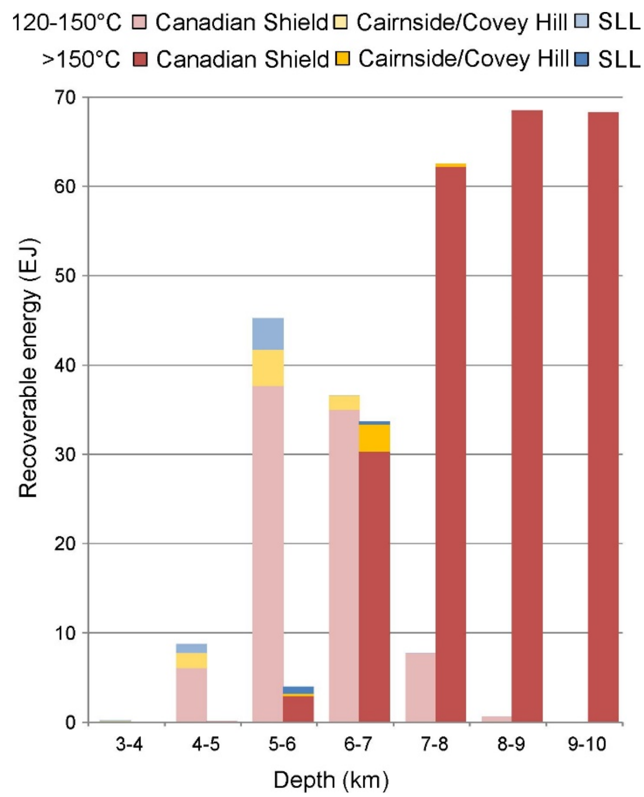

Figure 11. Recoverable energy considering a 20% recovery factor for the thermal units above 120 °C. SSL: sedimentary units with potential reservoir characteristics without the Cairnside and Covey Hill thermal units.

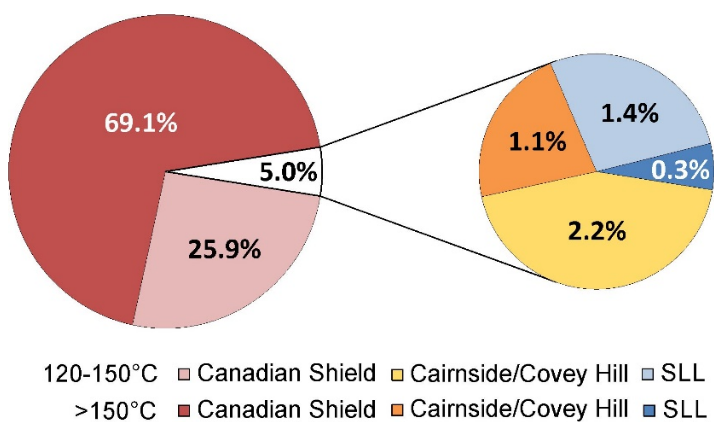

Figure 12. Distribution of the recoverable geothermal energy down to 10 km depth in the different thermal units. SSL: sedimentary units with potential reservoir characteristics without the Cairnside and Covey Hill thermal unit.

The electrical power estimated in the context of a binary power plant with 30 years exploitation period is on the order of 45,000 MWe for all the thermal units with potential reservoir characteristics and the basement above 120 °C, when considering a recovery factor of 20%. This is similar to the total electrical power actually installed in the Province of Québec (Table 2). The electrical power estimated with a 2% recovery factor is consequently

4500 MWe, which is similar to the hydroelectric power plant of Churchill Falls (Table 2). More precisely, the electrical power associated with the combined Cairnside and Covey Hill thermal unit above 150 °C is mainly available between 6 and 7 km depth and is on the order of 400 and 40 MWe, considering a recovery factor of 20% and 2%, respectively.

Table 2. Power generation in the Province of Québec (Hydro-Québec, 2017).

Power plant capacity at the end of 2017	**MW**
Hydroelectric power plants (70)	36,874
Churchill Falls power plant (Labrador)	5,428
Wind farms (39)	3,508
Thermal plants (24)	542
Biomass and biogas cogeneration plants (12)	272
Others	988
Total	**47,612**

5 Discussion and conclusions

The 3D temperature model presented in this paper was used to accurately assess geothermal resources of thermal units in the SLL, including the underlying Canadian Shield and considering the sedimentary basin architecture. The volume estimate was based on the number of 3D cells having the appropriate threshold temperatures of 120 °C and 150 °C, allowing to calculate the geothermal energy available in the SSL basin as function of temperature, depth and thermal unit distribution. Evaluation of energy content in each thermal unit as shown in Figure 11 is a new information for the SLL basin that could not have been obtained with previous 1D or 2D modeling approaches (Majorowicz and Minea, 2012; Bédard *et al*., 2017). The 3D geological model, incorporating analytical heat transfer solutions, is a powerful tool to rapidly compute geothermal resources and illustrate which thermal units contains the energy, at what depth and where. In the 3D model, only 5 % of the total geothermal resource that is appropriate for power generation (25,000 EJ) is located in the SSL basin units with potential reservoir characteristics at depth greater than 4 km. Consequently, the vast majority of the geothermal resources for power generation is located in the Canadian Shied, which is not considered as a conventional reservoir rock and, therefore, implies the use of EGS. Reservoir stimulation appears a key to unlock deep geothermal resources of the SLL basin. This shows the added value of a geothermal resource estimated based on a 3D geological model, offering more information on resource location, a significant advance compared to previous 1D and 2D geothermal resources assessments (Majorowicz and Minea, 2012; Bédard *et al*., 2017).

The use of a 3D regional geological model, in which steady-state conductive heat transfer equations have been implemented, brings resource quantification to a high level and was proven valuable to identify regional targets with geothermal resources at shallower depth. The evaluation of temperature distribution revealed two anomalies with a higher temperature at shallower depth, when compared to the basin average temperature distribution, and therefore greater geothermal potential. As the Cairnside and Covey Hill thermal units show the higher porosity of the sedimentary sequence, they represent, together with the potentially fractured basement at the basin interface, the most suitable target for geothermal exploration. The AE anomaly appears to be the area of interest to explore for hydrothermal resources for power generation as this is the only region where the sedimentary rocks of the Cairnside and Covey Hill can reach temperatures of 150 °C and more. On the other hand, in the SOM anomaly, the temperature reaches 120 °C at a shallower depth, between 3,500 and 4,000 m, but in the Precambrian basement because the sedimentary basin is thinner. The SOM anomaly, thus, represents a target for EGS exploration. Again, the above information was inferred from the results of 3D geological modeling that is thought to better evidence resource depth, magnitude and location (Figure 11).

The geological model was based on data from 81 oil and gas exploration wells, the surface geological map and geophysical interpretations that are sparse and heterogeneously distributed both over the entire model area and at depth (Bédard *et al.*, 2013). A large uncertainty with respect to temperature prediction is therefore expected for the 3D model where data are sparse, especially near the SOM anomaly (Figure 6). In general, the density of available well data decreases toward the southeastern and deeper part of the basin.

Moreover, input temperature obtained from corrected BHT is the main source of uncertainty related to the evaluation of temperature at depth (Bédard *et al*., 2017). Those are not equilibrium temperature and the two anomalies discussed in this manuscript are both based on one BHT data that could not be validated or invalidated and were therefore included in the temperature model evidencing the present target anomalies when interpolating the surface heat flow (Figure 4 and 6). Ranges of thermal conductivity and internal heat generation was previously identified for each thermal unit by *Bédard et al.* (2017) based on the statistical distribution of laboratory and borehole analysis. Heat flow was consequently estimated for pessimistic and optimistic scenarios, showing an average variation of

± 35 mW m^{-2}, which is more than the kriging standard deviation (Figure 6). The uncertainty of the resulting temperature prediction increases downward. The temperature uncertainty at 10 km depth is about 18 °C while it is less than 10 °C at less than 7 km depth when considering plausible thermal property scenarios. It is important to note that BHT density additionally decreases with depth. Nevertheless, this does not impact the method highlighted in this contribution to assess geothermal resources of sedimentary basins with a regional 3D model. Of course, the quantity of available geothermal resources can be affected by the accuracy of the temperature prediction that is subject to BHT correction and thermal property uncertainties, but the location of thermal anomalies is expected to remain the same regardless of in input parameter variability. This comprehensive resource assessment can be seen as a first step to justify expenses to collect equilibrium temperature data in deep wells, which can be integrated to the 3D temperature model to reduce its uncertainty as the stage of geothermal exploration moves one step further in the SLL. For example, equilibrium temperature data have been used in the Williston basin to help correct BHT and predict temperature of basal formations in 3D (Gosnold et al., 2016). In this case, the extrapolation of temperature was done vertically; taking into account the thermal stratigraphy but the temperature was interpolated in 3D space without building a geological model. A next sept is definitely to combine equilibrium temperature data with a 3D geological model to refine regional geothermal resource assessment of sedimentary basins. For the SLL basin, this can be the opportunity to validate the existence of the modelled temperature anomalies.

The integration of steady-state conductive heat transfer equations in a 3D geological model, first achieve for the SLL basin to analytically compute temperature at a regional scale and evaluate geothermal resource distribution, appears to be a significant scientific development. Recent studies to estimate geothermal resources on a regional scale with the same analytical heat conduction method were often based on a 2D mapping approaches (Batir *et al*., 2016; Stutz *et al.*, 2015; Palmer-Wilson *et al.*, 2018). The surface heat flow map is seen as the baseline information to estimate temperature at depth with downward extrapolation assuming a uniform subsurface thermal conductivity in the crust (Blackwell *et al.*, 2006; Majorowicz and Minea, 2012). The use of a 3D model allowed to compute the equivalent thermal properties as function of depth, which are affected by the distribution of thermal units and the basin architecture further influencing temperature and resource estimates. The surface heat flow distribution still remained the baseline information in this study, but the extrapolation of temperature at depth was based on a representative conceptualization of the geological units considering thermal properties changing according to unit geometry (Figure 3). Additionally, simple kriging with calculation of the standard deviation was used in this study to interpolate heat flow data at surface and evaluate uncertainty, which is one step further from previous assessments showing interpolation results only (Blackwell *et al.*, 2006; Majorowicz and Minea, 2012; Gosnold *et al.*, 2016; Palmer-Wilson *et al.*, 2018). The map of surface heat flow standard deviation allows to rapidly identify where data is missing and more work should be conducted to validate or invalidate potential anomalies.

This estimation of geothermal resources based on a 3D geological model would not have been possible without a previous assessment of thermal unit properties (Bédard *et al.*, 2017). Laboratory measurements of thermal conductivity for rock samples of each unit (Nasr *et al.*, 2015; Nasr, 2016) and well log analysis to define internal heat generation rates are prior information that may not be available in all regional geothermal resource assessment, but essential to make appropriate use of the 3D model. Indeed, a fine regional understanding of geological setting combined to a detail thermal unit characterization is needed to process with the proposed methodology. Similar work has been achieved in the French Massif Central by Calcagno *et al.* (2014) and in Denmark by Fuchs *et al.* (2020), but with notable differences in the methodology. These authors meshed their 3D geological model to conduct a numerical simulation of steady-state heat conduction using the finite element method to determine temperature in the 3D space. Numerical simulations generally imply iterative computations providing approximate solutions that can be meshed sensitive, has to be done with additional software from that used to build the geological model and can require large computing time. On the other hand, analytical calculations done for the present work implies an exact solution that is not sensitive to the shape of mesh elements and can be carried directly in the 3D geological model with short computation time. However, the numerical approach provides a true 3D heat transfer simulation while the analytical approach is more easily computed with 1D conductive heat transfer (vertical), but constrained from the 3D geological architecture. Both methods have advantages and disadvantages that can be weighted to decide on the methodology to put forward when estimating geothermal resources at the regional scale.

The assessment of the geothermal resources of the SLL basin was done for power generation purposes targeting host rocks with temperature above 120 °C. Only a small portion of the potential resource is located in the SLL basin units and is, moreover, located at more than 4 km depth where the temperature uncertainty is important. The use of such low-temperature geothermal resources for power generation implies deep exploration and production drilling with consequent investment. Given the depth of geothermal resources for power generation, the direct use of heat can be an attractive option for future geothermal development in the context of the Province of Québec, where the electricity is dominantly produced by hydroelectric power plants and is widely available at low price while space heating needs remain important due to the cold climate. Further work can be done with a direct use perspective to identify thermal units above 60 °C that is hot enough to be used for space heating or other applications. The proximity of geothermal resources suitable for direct use with respect to population center will have to be highlighted in this next step.

6 Acknowledgements

The *Fonds de recherche du Québec – Nature et technologies* (FRQNT) and the *Institut de recherche d'Hydro-Québec* are acknowledged for funding this research. The third author was supported by a Banting scholarship during the completion of this research.

On behalf of all authors, the corresponding author states that there is no conflict of interest.

7 References

Batir, J.F., Blackwell, DD., Richards, M.C., 2016. Heat Flow and Temperature-Depth Curves Throughout Alaska: Finding Regions for Future Geothermal Exploration. Journal of Geophysics and Engineering 13 (3), 366–78. https://doi.org/10.1088/1742-2132/13/3/366.

Bédard, K., Comeau, F.-A., Millet, E., Raymond, J., Malo, M., Gloaguen, E., 2016. Évaluation des ressources géothermiques du bassin des Basses-Terres du Saint-Laurent. Institut national de la recherche scientifique. Report R1659, Québec. http://espace.inrs.ca/4845/.

Bédard, K., Comeau, F.-A., Raymond, J., Malo, M., Nasr, M., 2017. Geothermal Characterization of the St. Lawrence Lowlands Sedimentary Basin, Québec, Canada. Natural Resources Research, 27, 479-502. https://doi.org/10.1007/s11053-017-9363-2.

Bédard, K., Malo, M., Comeau, F.-A., 2013. CO_2 Geological Storage in the Province of Québec, Canada Capacity Evaluation of the St. Lawrence Lowlands basin. Energy Procedia, 37, 5093-5100. http://dx.doi.org/10.1016/j.egypro.2013.06.422.

Bédard, K., Raymond, J., Malo, M., Konstantinovskaya, E., Minea, V., 2014. St. Lawrence Lowlands bottom-hole temperatures: various correction methods. GRC Transactions, 38, 351-355.

Békési, E., Struijk, M., Bonté, D., Veldkamp, H., Limberger, J., Fokker, P.A., Vrijlandt, M., van Wees, J-D., 2020. An updated geothermal model of the Dutch subsurface based on inversion of temperature data. Geothermics, 88, 101880. https://doi.org/10.1016/j.geothermics.2020.101880.

Bertrand, R, Chagnon, A., Malo, M., Duchaine, Y., Lavoie, D., Savard, M.M., 2003. Sedimentologic, Diagenetic and Tectonic Evolution of the Saint-Flavien Gas Reservoir at the Structural Front of the Quebec Appalachians. Bulletin of the Canadian Petroleum Geology, 51 (2), 126–54. https://doi.org/10.2113/51.2.126.

Blackwell, D.D., Negraru, P., Richards, M., 2006. Assessment of the Enhanced Geothermal System Resource Base of the United States. Natural Resources Research, 15 (4), 283-308. http://dx.doi.org/10.1007/s11053-007-9028-7.

Blackwell, D.D., Richards, M., (2004) Geothermal map of North America. American Association of Petroleum Geologists, sheet 1, scale 1:6,500,000.

Blöcher, M.G., Zimmermann, G., Moeck, I., Brandt, W., Hassanzadegan, A., Magri, F., 2010. 3D Numerical Modeling of Hydrothermal Processes during the Lifetime of a Deep Geothermal Reservoir. Geofluids 10 (3): 406–21. https://doi.org/10.1111/j.1468-8123.2010.00284.x.

Calcagno, P., Baujard, C., Guillou-Frottier, L., Dagallier, A., Genter, A., 2014. Estimation of the deep geothermal potential within the Tertiary Limagne Basin (French Massif Central): An integrated 3D geological and thermal approach. Geothermics, 51, 496-508. http://dx.doi.org/10.1016/j.geothermics.2014.02.002.

Canadian GeoExchange Coalition (2012) The state of the Canadian geothermal heat pump industry 2011 - Industry survey and market analysis. Canadian Geoexchange Coalition. Internal report, Montréal.

Castonguay, S., Lavoie, D., Dietrich, J., Laliberté, J.-Y., 2010. Structure and petroleum plays of the St. Lawrence Platform and Appalachians in southern Quebec: insights from interpretation of MRNQ seismic reflection data. Bulletin of Canadian Petroleum Geology, 58 (3), 219-234. http://dx.doi.org/10.2113/gscpgbull.58.3.219.

Chang, P.-Y., Lo, W., Song, S.-R., Ho, K.-R., Wu, C.-S., Chen, C.-S., Lai, Y.-C., Chen, H.-F., Lu, H.-Y., 2014. Evaluating the Chingshui geothermal reservoir in northeast Taiwan with a 3D integrated geophysical visualization model. Geothermics, 50, 91-100. https://doi.org/10.1016/j.geothermics.2013.09.014.

Comeau, F.-A., Bédard, K., Malo, M., 2013. Lithostratigraphie standardisée du bassin des Basses-Terres du Saint-Laurent basée sur l'étude des diagraphies. Institut national de la recherche scientifique, Report R-1442 (INRSCO2-2013-V1.4), Québec. http://espace.inrs.ca/1645/.

Fuchs, S, Balling, N., Mathiesen, A., 2020. Deep basin temperature and heat-flow field in Denmark – New insights from borehole analysis and 3D geothermal modelling. Geothermics, 83, 101722. https://doi.org/10.1016/j.geothermics.2019.101722.

Gasperikova, E., Rosenkjaer, G.K., Arnason, K., Newman, G.A., Lindsey, N.J., 2015. Resistivity characterization of the Krafla and Hengill geothermal fields through 3D MT inverse modeling. Geothermics, 57, 246-257. https://doi.org/10.1016/j.geothermics.2015.06.015.

Gosnold, W., McLaughlin, S., Colby, C., 2016. Preliminary Three-Dimensional Temperature Structure of the Williston Basin. GRC Transcations 40:639–42.

Guglielmetti, L., Comina, C., Abdelfettah, Y., Schill, E., Mandrone, G., 2013. Integration of 3D geological modeling and gravity surveys for geothermal prospection in an Alpine region. Tectonophysics, 608, 1025-1036. https://doi.org/10.1016/j.tecto.2013.07.012.

Guillou-Frottier, L., Mareschal, J.-C., Jaupart, C., Gariépy, C., Lapointe, R., Bienfait, G., 1995. Heat flow variations in the Grenville Province, Canada. Earth and Planetary Science Letters, 136 (3–4), 447-460. http://dx.doi.org/10.1016/0012-821X(95)00187-H.

Hofmann, H., Weides, S., Babadagli, T., Zimmermann, G., Moeck, I., Majorowicz, J., Unsworth, M., 2014. Potential for enhanced geothermal systems in Alberta, Canada. Energy, 69, 578-591. http://dx.doi.org/10.1016/j.energy.2014.03.053.

Hydro-Québec, 2017. Rapport annuel 2017. Public report, Motréal. www.hydroquebec.com/a-propos/resultats-financiers/rapport-annuel.html.

Jessop, A.M., 1990. Thermal geophysics. Elsevier. Amsterdam, The Netherlands. http://dx.doi.org/10.1016/B978-0-444-88309-4.50015-4.

Konstantinovskaya, E., Rodriguez, D., Kirkwood, D., Harris, L.B., Thériault, R., 2009. Effects of Basement Structure, Sedimentation and Erosion on Thrust Wedge Geometry: An Example from the Quebec Appalachians and Analogue Models. Bulletin of Canadian Petroleum Geology, 57 (1), 34-62. http://dx.doi.org/10.2113/gscpgbull.57.1.34.

Lachenbruch, A.H., 1970. Crustal temperature and heat production: Implications of the linear heat-flow relation. Journal of Geophysical Research, 75 (17), 3291-3300. http://dx.doi.org/10.1029/JB075i017p03291.

Lefebvre, P., Trempe, R., 1980. Gradient géothermique dans les Basses-Terres. Ministère des Ressources naturelles et de la Faune, Rapport #9206, 1980TA000-01, Québec.

Majorowicz, J., Minea, V., 2012. Geothermal energy potential in the St-Lawrence River area, Québec. Geothermics, 43, 25-36. http://dx.doi.org/10.1016/j.geothermics.2012.03.002.

Majorowicz, J., Minea, V., 2015a. Geothermal Energy Potential in Low Enthalpy Areas as a Future Energy Resource: Identifying Feasible Targets, Quebec, Canada, Study Case. Resources, 4 (3), 524.

Majorowicz, J., Minea, V., 2015b. Shallow and deep geothermal energy potential in low heat flow/cold climate environment: northern Québec, Canada, case study. Environmental Earth Sciences, 74 (6), 5233-5244. http://dx.doi.org/10.1007/s12665-015-4533-1.

Mareschal, J.C., Pinet, C., Gariépy, C., Jaupart, C., Bienfait, G., Coletta, G.D., Jolivet, J., Lapointe, R., 1989. New heat flow density and radiogenic heat production data in the Canadian Shield and the Quebec Appalachians. Canadian Journal of Earth Sciences, 26 (4), 845-852. http://dx.doi.org/10.1139/e89-068.

MIT, 2006. The future of geothermal energy. Impact of enhanced geothermal systems (EGS) on the United States in the 21st century. Massachusetts Institute of Technology, Idaho National Laboratory. INL/EXT-06-11746.

Nasr, M., Raymond, J., Malo, M., 2015. Évaluation en laboratoire des caractéristiques thermiques du bassin sédimentaire des Basses-terres du Saint-Laurent. Proceedings of the 68th Canadian Geotechnical Conference and 7th Canadian Permafrost Conference, Québec.

Nasr, M. (2016) Évaluation des propriétés thermiques de la Plate-forme du Saint-Laurent : Mesures au laboratoire et approche diagraphique. Institut National de la Recherche Scientifique, M.Sc. Thesis, Québec. http://espace.inrs.ca/4637.

Nasr, M., Raymond, J., Malo, M. et Gloaguen, E. (2018) Geothermal potential of the St. Lawrence Lowlands sedimentary basin from well log analysis. Geothermics, 75, 68-80. https://doi.org/10.1016/j.geothermics.2018.04.004.

Newman, G.A., Gasperikova, E., Hoversten, G.M., Wannamaker, P.E., 2008. Three-Dimensional Magnetotelluric Characterization of the Coso Geothermal Field. Geothermics 37 (4), 369–99. https://doi.org/10.1016/j.geothermics.2008.02.006.

Nieto, I.M., Martín, A.F., Blázquez, C.S., Aguilera, D.G., García, P.C., Vasco, E.F., and García, J.C., 2019. Use of 3D Electrical Resistivity Tomography to Improve the Design of Low Enthalpy Geothermal Systems. Geothermics 79, 1–13. https://doi.org/10.1016/j.geothermics.2019.01.007.

Palmer-Wilson, K., Banks, J., Walsh, W., Robertson, B., 2018. Sedimentary Basin Geothermal Favourability Mapping and Power Generation Assessments. Renewable Energy 127: 1087–1100. https://doi.org/10.1016/j.renene.2018.04.078.

Przybycin, A.M., Scheck-Wenderoth, M., Schneider, M., 2017. The origin of deep geothermal anomalies in the German Molasse Basin: results from 3D numerical models of coupled fluid flow and heat transport. Geothermal Energy, 5, 1. http://dx.doi.org/10.1186/s40517-016-0059-3.

Ratouis, T.M.P., O'Sullivan, M.J., O'Sullivan, J.P., 2016. A Numerical model of Rotorua Geothermal Field. Geothermics, 60, 105-125. https://doi.org/10.1016/j.geothermics.2015.12.004.

Raymond, J., Malo, M., Comeau, F.-A., Bedard, K., Lefebvre, R., Therrien, R., 2012. Assessing the geothermal potential of the St. Lawrence sedimentary basin in Québec, Canada. 39th IAH Congress, Niagara Falls.

Raymond, J., Sirois, C., Nasr, M., Malo, M., 2017. Evaluating the Geothermal Heat Pump Potential from a Thermostratigraphic Assessment of Rock Samples in the St. Lawrence Lowlands, Canada. Environmental Earth Sciences 76 (2), 83. https://doi.org/10.1007/s12665-017-6398-y.

Santilano, A., Donato, A., Galgaro, A., Montanari, D., Menghini, A., Viezzoli, A., Di Sipio, E., Destro, E., Manzella, A., 2016. An integrated 3D approach to assess the geothermal heat-exchange potential: The case study of western Sicily (southern Italy). Renewable Energy, 97, 611-624. https://doi.org/10.1016/j.renene.2016.05.072.

Saull, V.A., Clark, T.H., Doig, R.P., Butler, R.B., 1962. Terrestrial heat flow in the St. Lawrence Lowland of Quebec. Canadian Mining and Metallugicical Bulletin, 65, 63-66.

Sausse, J., Dezayes, C., Dorbath, L., Genter, A., Place., J., 2010. 3D Model of Fracture Zones at Soultz-Sous-Forêts Based on Geological Data, Image Logs, Induced Microseismicity and Vertical Seismic Profiles. Vers l'exploitation des ressources géothermiques profondes des systèmes hydrothermaux convectifs en milieux naturellement fracturés 342 (7): 531–45. https://doi.org/10.1016/j.crte.2010.01.011.

Siler, D.L., Faulds, J.E., Mayhew, B., McNamara, D.D., 2016. Analysis of the favorability for geothermal fluid flow in 3D: Astor Pass geothermal prospect, Great Basin, northwestern Nevada, USA. Geothermics, 60, 1-12. https://doi.org/10.1016/j.geothermics.2015.11.002.

Siler, D.L., Faulds, J.E., Hinz, N.H., Dering, G.M., Edwards, J.H., and Mayhew, B., 2019. Three-Dimensional Geologic Mapping to Assess Geothermal Potential: Examples from Nevada and Oregon. Geothermal Energy 7, 2. https://doi.org/10.1186/s40517-018-0117-0.

SNC-SOQUIP, 1979. Rapport sur le potentiel en énergie géothermique de basse énergie dans les Basses Terres du St-Laurent. Ministère des Ressources Naturelles et de la Faune, Report 1979TA000-04, Québec.

Srivastava, R.M., 1994. An overview of stochastic methods for reservoir characterization. In: Yarus, J.M., Chambers, R.L. [eds], Stochastic modeling and geostatistics - Principle, methods, and case studies. AAPG computer Application in geology, No. 3. American Association of Petroleum Geologists, Tulsa.

Stein, C.A., 1995. Heat Flow of the Earth. In: Ahrens, T.J. [ed.], Global Earth Physics. American Geophysical Union, Washington D.C. http://dx.doi.org/10.1029/RF001p0144.

Stutz, G.R., Shope, E., Jordan, T.E., Reber, T.J., Whealton, C.A., Aguirre, G.A., Smith, J.D., et al. 2015. Geothermal Energy Characterization in the Appalachian Basin of New York and Pennsylvania. Geosphere 11 (5), 1291–1304. https://doi.org/10.1130/GES00499.1.

Tran Ngoc, T.D., Lefebvre, R., Konstantinovskaya, E., Malo, M., 2014. Characterization of Deep Saline Aquifers in the Bécancour Area, St. Lawrence Lowlands, Québec, Canada: Implications for CO2 Geological Storage. Environmental Earth Sciences 72 (1): 119–46. https://doi.org/10.1007/s12665-013-2941-7.

Turcotte, D.L., Schubert, G., 2014. Geodynamics. Third Edition, Cambridge University Press, Cambridge.

Williams, C.F., Reed, M.J., Mariner, R.H., 2008. A review of methods applied by the U.S. Geological Survey in the assessment of identified geothermal resources. U.S. Geological Survey, Open File Report 2008-1296.

Zhao, Y., Feng, Z., Feng, Z., Yang, D., Liang, W., 2015. THM (Thermo-Hydro-Mechanical) Coupled Mathematical Model of Fractured Media and Numerical Simulation of a 3D Enhanced Geothermal System at 573 K and Buried Depth 6000–7000 M. Energy 82, 193–205. https://doi.org/10.1016/j.energy.2015.01.030.